# Microstructure evolution and age-hardening response in Mg-Sn-Sm alloys under a wide range of Sm/Sn ratio

***Feng Liu[1, 2], **Wen-xin Hu[1, 2], Zheng-hua Yang[1, 2], Wei Wang[2], and Wei He[2]**

*1. State Key Laboratory of Baiyunobo Rare Earth Resource Researches and Comprehensive Utilization, Baotou 014030, Inner Mongolia, China*

*2. Baotou Research Institute of Rare Earths, Baotou 014030, Inner Mongolia, China*

**Abstract:** The microstructure evolution and age-hardening response for different Sm/Sn ratios (0–2.55, in wt.%) of Mg-Sn-Sm alloys were investigated. The second phase formation in as-cast alloys and the $Mg_3Sm$ precipitates formed in aged alloys were characterized using XRD, FESEM and HAADF-STEM with EDS techniques. Results indicate that the Sm/Sn ratio has a great influence on the phase constitution, α-Mg grain size and age-hardening response. With the increment of Sm/Sn ratio, $Mg_{41}Sm_5$ and thermally stable MgSnSm phases precipitate. When the Sm/Sn ratio is about 1.19, the secondary dendrite arm spacing of α-Mg grains significantly decreases. Furthermore, the alloy with Sm/Sn ratio up to 2.55 exhibits the highest age-hardening response, the hardness value increases from 52 HB at solution-treated condition to 74 HB at peak-aged condition (ageing at 220 °C for a short time of 4 h). This is attributed to the large volume fraction of needle-like $Mg_3Sm$ precipitates formed in the α-Mg matrix during ageing treatment, which results in a significant precipitation strengthening effect.

**Keywords:** magnesium alloy; as-cast; microstructure evolution; age-hardening; precipitates; Sm/Sn ratio

**CLC numbers:** TG146.22 **Document code:** A **Article ID:** 1672-6421(2022)03-211-07

## 1 Introduction

Magnesium is the lightest structural metal and offers tremendous weight saving potential. However, current commercial magnesium alloys still suffer from inadequate strength and creep resistance. Thus, enhancing the mechanical properties of magnesium alloys is an essential requirement for expanding their applications [1, 2]. The Mg-Sn based magnesium alloys are known as a precipitation strengthening system and have received considerable attention [3, 4]. As-cast binary Mg-Sn alloys mainly consist of α-Mg and equilibrium precipitate phase $Mg_2Sn$. The solubility of Sn in magnesium is 14.5wt.% at the eutectic temperature of 561 °C, and it sharply drops to ~0.45wt.% at 200 °C, which provides the basis for precipitation strengthening during ageing treatment. What is more, the intermetallic phase $Mg_2Sn$ in Mg-Sn alloys has a much higher melting point of 770 °C than the $Mg_{17}Al_{12}$ phase of 462 °C in Mg-Al alloys. Thus, Mg-Sn based alloys are likely to obtain excellent thermal stability at elevated temperatures [5].

Either small or large quantities of ternary and quaternary alloying elements have been added into the Mg-Sn based alloys in the past years to enhance their mechanical properties. Nayyeri et al. [6] investigated the effect of Ca addition on the microstructure stability and mechanical properties of Mg-5Sn alloy, and suggested that the high volume fraction of thermally stable CaMgSn precipitates contributed to the retention of the ultimate shear strength and hardness by hindering grain growth during the annealing process. Li et al. [7] found that the combined addition of Ca and Ag in Mg-7Sn alloy has a positive effect on grain refinement from 113.5 μm to 54.3 μm, and the peak-aged hardness value increases from 61.1 HV to 80.4 HV after ageing treatment at 200 °C. The rare earth (RE) elements are well known to strengthen the magnesium alloys through formation of the rare earth precipitates produced during solidification process or ageing treatment. The solidification behavior of Mg-Sn-Y alloys has been studied by Muthuraja et al [8], and they pointed out that Mg-Sn-Y alloys are promising creep resistance alloys for high temperature applications because the highly stable $Sn_3Y_5$ phase (melting point:

***Feng Liu**

Male, born in 1990, Master. His research interests mainly focus on the microstructures and mechanical properties of magnesium alloys.

E-mail: liufeng9016@126.com

****Wen-xin Hu**

E-mail: Brirehuwenxin@126.com

**Received: 2021-06-19; Accepted: 2021-12-01**

1,940 °C) is in equilibrium with α-Mg phase. Yang et al. [9] found that the addition of 1.5wt.% or 2.0wt.% Ce efficiently refines the size of CaMgSn phase in Mg-3Sn-2Ca alloy and leads to the enhancement of tensile and anti-creep properties. What is more, they reported that particle-like shaped MgSnY and GdMgSn phases were formed when sufficient Y and Gd were added into the Mg-3Sn-2Ca alloy, respectively [10, 11]. Chen et al. [12] suggested that the appropriate addition of Y to Mg-5Sn-3Zn can refine the grains and promote the precipitation of MgSnY phase with high stability. Recently, Wang et al. [13] found that Sc is beneficial for both the grain refinement and modification of secondary phase morphology in the as-cast Mg-4.5Sn-5Zn alloy. Samarium (Sm) has a relatively high solid solubility in α-Mg matrix, which decreases with a reduction in temperature, thus, Sm is considered as a promising alternative to optimize the performance of magnesium alloys via precipitation strengthening. In addition, Sm is one of the least expensive light RE elements, from the perspective of cost, Sm also has a great potential for future industrial application in magnesium alloys than those expensive Y, Gd and Sc elements [14]. However, the effect of Sm addition on the as-cast microstructure evolution and age-hardening nature of Mg-Sn based alloys is rarely reported.

The aim of this study is to investigate the microstructure evolution and age-hardening response of as-cast and aged Mg-Sn-Sm alloys under a wide range of Sm/Sn ratios (within 0–2.55, in wt.%), and the precipitation strengthening mechanisms were elucidated. It is expected that the results can be helpful in future design and optimization of the Mg-Sn-Sm alloy system.

## 2 Experimental procedure

The raw materials consisted of commercial pure Mg, pure Sn and Mg-35Sm master alloy. The pure Mg was melted in an electric resistance furnace using a steel crucible under a mixed protective gas of $SF_6$ (50 mL·min$^{-1}$) and $N_2$ (5 L·min$^{-1}$), the preheated Sn and Mg-35Sm master alloy were added to the melt at 680 °C with designed content, and then the alloy melt was manually stirred for about 10 min at 730 °C, subsequently held for another 20 min to ensure the complete dissolution of elements in the melt. After deslagging, the melts were poured into a cast iron mold at room temperature to obtain Mg-Sn-Sm ingots with a diameter of 20 mm and a length of 130 mm with different Sm/Sn ratios. All alloy compositions were described in wt.%, and the Sm/Sn ratios were also described in weight ratio. After casting, the alloy ingots were solution-treated in a furnace protected with Ar atmosphere at 490 °C for 30 h, and then water quenched to room temperature. The ageing process was performed in a furnace at 220 °C for various times from 1 h to 1,000 h.

Metallographic specimens were cut from the central parts along the axes of rod ingots and then grounded and polished in accordance with standard procedures used for metallographic preparation of metal samples. The chemical composition analysis was carried out using inductively couple plasma-atomic emission spectroscopy (ICP-AES), and the results are listed in Table 1. Microstructures were observed using optical microscopy (OM) and field emission scanning electron microscopy (FESEM, Zeiss-SIGMA500) equipped with an energy dispersive spectrum (EDS, Bruker-xFlash 6160) analyzer. The phase constitutions were analyzed by X-ray diffraction (XRD, X-pertpowder) using Cu Kα radiation in step mode from 20° to 80° with a scanning speed of 4°·min$^{-1}$. The hardness of samples was measured using a Brinell hardness tester under a load force of 2,452 N and dwelling time of 30 s. At least five indents per sample were analyzed and the average value was reported as the hardness. Thin foils used for TEM observation were prepared by mechanical polishing (~70 μm), and then ion-milled by Gatan Precision Ion Polishing System (PIPS, GATAN 695) with 3.0 kV ion gun energy and 2° milling angle. The transmission electron microscopy (TEM) and high-angle annular dark-field scanning transmission electron microscopy (HAADF-STEM) analysis were performed by Talos F200i equipped with an EDS (Bruker-xFlash 6TI30) operating at 200 kV to study the structure of precipitates.

## 3 Results and discussion

### 3.1 Microstructure analysis of as-cast and solution-treated alloys

Figure 1 shows the optical micrographs of the as-cast Mg-Sn-Sm alloys. It can be seen from Fig. 1(a) that the TE0 alloy mainly consists of coarse dendritic α-Mg grains and the secondary phases along grain boundaries. According to the XRD result shown in Fig. 2(a), the second phase distributed along grain boundaries can be identified as $Mg_2Sn$. Figure 1(b) shows that some discontinuous secondary phases appear along the grain boundaries in TE1 alloy, meanwhile, α-Mg grains still exhibit as

**Table 1: Chemical composition of as-cast experimental alloys**

| Alloy No. | Alloying elements (wt.%) | | | Sm/Sn ratio |
|---|---|---|---|---|
| | Sn | Sm | Mg | |
| TE0 | 2.85 | 0 | Bal. | 0 |
| TE1 | 3.10 | 0.52 | Bal. | 0.17 |
| TE2 | 2.94 | 3.50 | Bal. | 1.19 |
| TE3 | 3.20 | 8.15 | Bal. | 2.55 |

dendrites. Nevertheless, when the ratio of Sm/Sn increases to 1.19 in TE2 alloy, the secondary dendrite arm spacing of α-Mg grains decreases significantly, as shown in Fig. 1(c), which indicates that the appropriate ratio of Sm/Sn can effectively refine the grain size of the as-cast Mg-Sn-Sm alloy. RE element addition is generally considered as an effective way to refine grains of the as-cast magnesium alloys [15, 16]. In this study, the segregation of Sm atoms ahead of the growing α-Mg dendrites decreases the solid-liquid interface energy, thus restricts the growth of the α-Mg dendrites. What is more, Sm has a relatively larger growth restricting factor (GRF) among the RE elements, which relies on the solute concentration [17], it tends to build up constitutional cooling in front of the solid-liquid interface. The high content of Sm increases the GRF, which would hinder the dendrite growth, thus results in the remarkable refinement of grains. When the ratio of Sm/Sn further increases to 2.55 in TE3 alloy [Fig. 1(d)], a large volume fraction of rod-like and needle-like phases appear both in grains and at the grain boundaries. The XRD results in Figs. 2(b)–(d) further demonstrate that the $Mg_{41}Sm_5$ phase appears with the increasing ratio of Sm/Sn. In addition, when the Sm/Sn ratio reaches as high as 2.55, the $Mg_2Sn$ phase can barely be found in TE3 alloy.

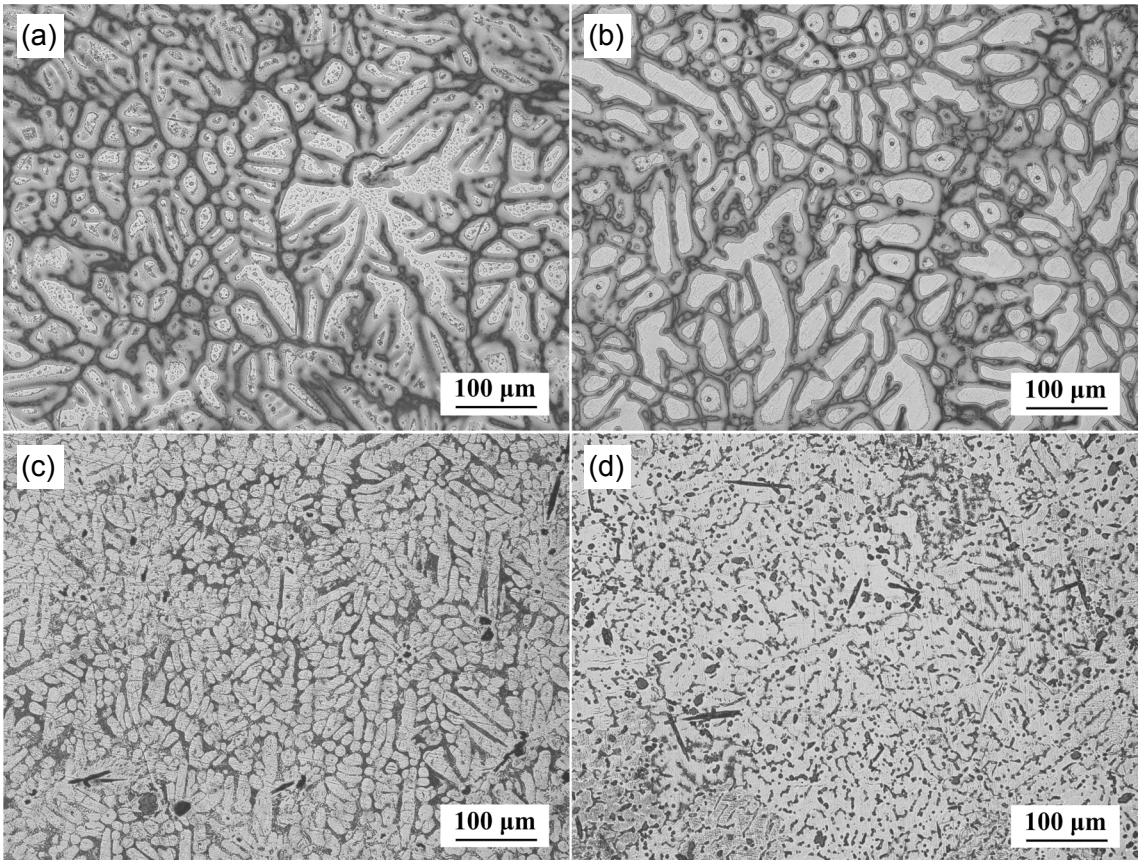


**Fig. 1: Optical microstructures of as-cast alloys: (a) TE0; (b) TE1; (c) TE2; and (d) TE3**

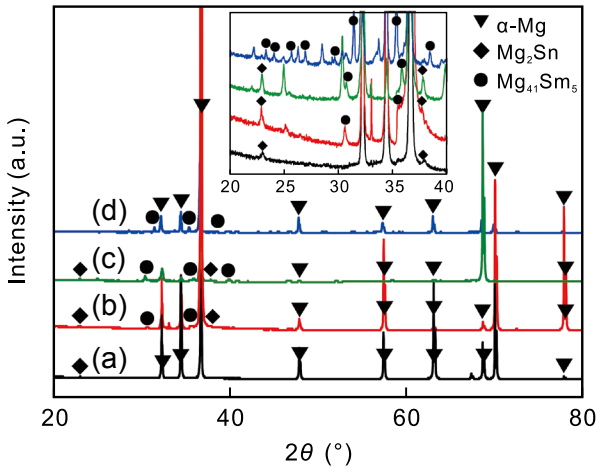


**Fig. 2: XRD patterns of as-cast alloys: (a) TE0; (b) TE1; (c) TE2; (d) TE3**

Figure 3 shows the microstructures of the experimental alloys solution-treated at 490 °C for 30 h. The $Mg_2Sn$ phase along the grain boundaries in TE0 alloy can be seen scarcely, as shown in Fig. 3(a). Nevertheless, some thermally stable second phases that cannot be dissolved into the matrix during the solution treatment are still observed clearly in TE1, TE2 and TE3 alloys, as shown by the arrows in Figs. 3(b)–(d).

Figure 4 shows the SEM images of the solution-treated TE1, TE2 and TE3 alloys. EDS results indicate that both the undissolved dot-like phase (marked by Arrow 1) in TE1 alloy and the feather-like phase (marked by Arrow 3) in TE2 alloy contained Mg, Sn and Sm elements, and the atomic ratio of Sn:Sm is close to 1:1. In the case of relatively small precipitates, an exact quantification of the composition of the precipitates is difficult to identify due to the size and penetration depth of the electron beam. In addition, the existing diffraction

database of XRD for the ternary compounds consisting of Mg, Sn and Sm elements is limited. Thus, these small particles are referred as $Mg_x$(SnSm) phase. Meanwhile, according to the EDS analysis, the polygon-shaped phases (marked by Arrow 2 and Arrow 4) appeared in TE2 and TE3 alloys are still composed of Mg, Sn and Sm elements, and the atomic ratio of Mg:Sn:Sm is close to 1:1:1. Therefore, these polygon phases are concluded as MgSnSm phases. Similarly, the ternary MgSnCe, MgSnNd and MgSnY phases have also been previously reported by other research groups [18-20], and they are considered as high thermally stable phases, which lead to the undissolving behavior. It is noticeable that some residual $Mg_{41}Sm_5$ phases are retained in the solution-treated TE3 alloy, as shown in Fig. 4(c) (marked by Arrow 5), this is mainly due to the supersaturated solubility of Sm in α-Mg matrix, as demonstrated in Fig. 5, which impedes the solute atoms diffusion and decreases the degradation of $Mg_{41}Sm_5$ phases.

Figure 5 shows the content of Sn and Sm solutes in α-Mg matrix via EDS analysis after solution treatment of the experimental alloys. As can be found, the solubility of Sn and Sm in α-Mg matrix is significantly influenced by the Sm/Sn ratio. In general, the solubility of Sn decreases with the increase

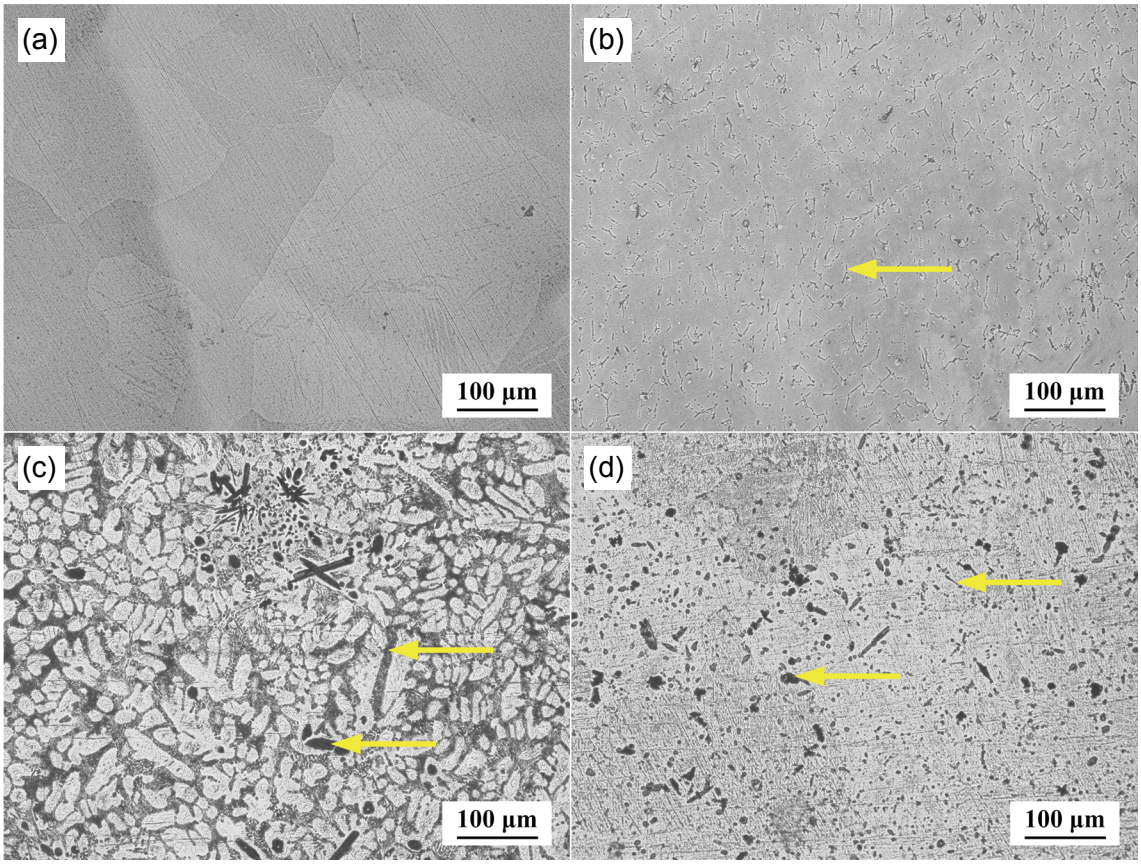


Fig. 3: Optical microstructure of alloys solution treated at 490 °C for 30 h: (a) TE0; (b) TE1; (c) TE2; and (d) TE3

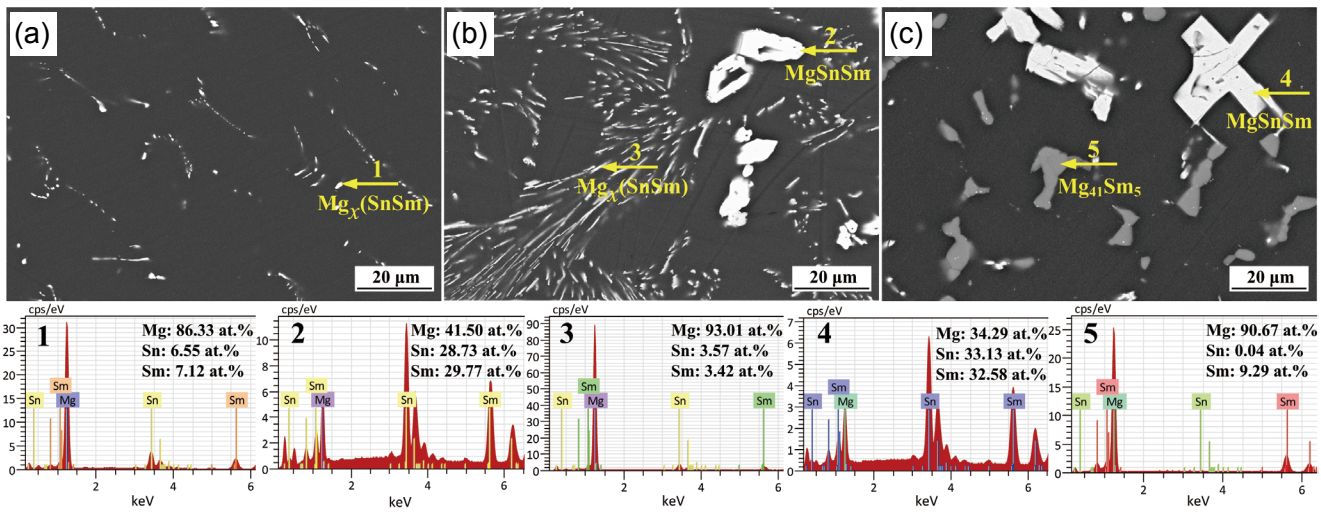


Fig. 4: SEM images of alloys solution treated at 490 °C for 30 h: (a) TE1; (b) TE2; and (c) TE3

of Sm/Sn ratio, this is due to the formation of the ternary $Mg_x$(SnSm) and MgSnSm phases during solidification process, which consumes a definite number of Sn atoms. In addition, both the solubility of Sn and Sm are extremely low in the TE2 alloy since a great numbers of Sn and Sm elements are consumed to form the $Mg_x$(SnSm) and MgSnSm compounds. It is worth noting that when Sm/Sn ratio increases up to 2.55 in the TE3 alloy, the solubility of Sm in α-Mg matrix reaches as high as 3.25wt.%, while no solubility of Sn is found. This is because due to the higher Sm/Sn ratio of TE3 alloy, the excess Sm content promotes the formation of a large quantity of $Mg_{41}Sm_5$ phases via a eutectic reaction similar to those in other Mg-RE systems, thus the dissolution of $Mg_{41}Sm_5$ phase during solution treatment contributes greatly to the significant increase of Sm concentration in α-Mg matrix. The aforementioned differences of solubility of Sn and Sm have a great influence on the later age-hardening response.

## 3.2 Effect of Sm/Sn ratio on age-hardening response

Figure 6 shows the age-hardening response of the experimental alloys after ageing treatment for various times at 220 °C. The age-hardening behaviors of these alloys suggest that the Sm/Sn ratio significantly affects the peak hardness values. According

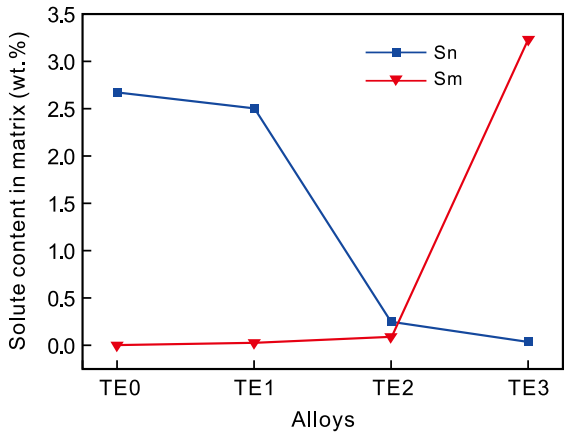


**Fig. 5: Solubility variations of Sn and Sm in α-Mg matrix after solution treatment**

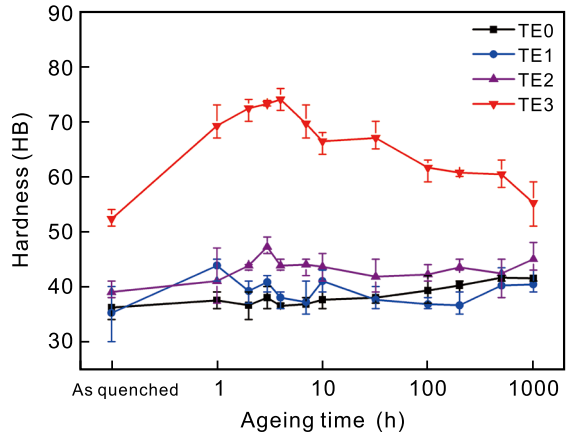


**Fig. 6: Age-hardening response of experimental alloys after aged at 220 °C for various times**

to the hardness curves in Fig. 6, the hardness values of solution-treated TE0, TE1 and TE2 alloys are almost the same (within the range from 35 HB to 39 HB). While the solution-treated TE3 alloy shows a comparatively higher hardness of 52 HB. This is mainly based on the following two reasons: on the one hand, a large volume fraction of undissolved $Mg_{41}Sm_5$ and MgSnSm phases result in dispersed hardening effect; on the other hand, the atomic size of Sm is much larger than Mg (more than 12% in diameter), hence, the large numbers of Sm atoms in α-Mg matrix of Mg-3Sn-8.2Sm alloy are likely to cause apparent solid-solution strengthening.

After ageing for as long as 500 h, the hardness of TE0 alloy shows a slight increment from 36 HB to a peak value of 42 HB, which is the lowest peak value in the four alloys. It is generally believed that $Mg_2Sn$ precipitates formed after isothermal ageing in Mg-Sn binary alloy exhibit coarse morphologies, they lie on the basal plane of the magnesium matrix and distribute heterogeneously, hence leads to the poor age-hardening response [21, 22]. However, the other three alloys with higher Sm/Sn ratios show a much shorter incubation period of age-hardening response, the hardness of TE1 and TE2 alloys rapidly reaches the peak values of 44 HB and 47 HB after ageing for 1 h and 3 h, respectively, but the percent increment of ageing hardness is not significant. This is ascribed to the fact that a high percentage of Sm element which plays an important role in ageing-hardening process is consumed to form the thermally stable $Mg_x$(SnSm) or MgSnSm compounds in the TE1 and TE2 alloys during solidification, as shown in Fig. 4(a) and Fig. 4(b), thus few Sm solute atoms (shown in Fig. 5) are dissolved into the α-Mg matrix during solution treatment to support the precipitating process, which weakens the ageing-hardening response. On the contrary, it is worth noting that a remarkable enhancement of hardness occurs in the TE3 alloy after ageing for 4 h, the hardness value increases from 52 HB to 74 HB, achieving a 42% increment. The peak hardness of TE3 alloy is the highest in these four alloys. According to Fig. 5, the solubility of Sm in the α-Mg matrix in TE3 alloy is considerably higher in comparison to the other three alloys. Sm is generally acknowledged as an effective ageing hardening element, hence, it is reasonable to deduce that the nonequilibrium situation in the supersaturated α-Mg solid solution provides the driving force for the precipitation of numerous Sm-containing phase, which is beneficial to improve the hardness value significantly during ageing process in TE3 alloy.

To gain a deeper insight into the precipitates in the peak-aged (aged at 220 °C for 4 h) TE3 alloy, HAADF-STEM observations were conducted, as shown in Fig. 7. Based on the low-magnification image shown in Fig. 7(a), it is visible that a large amount of needle-like precipitates distribute uniformly in the α-Mg matrix, the width of each needle-like precipitate is about 20 nm while the length varies in a large range. The magnified image of the precipitates is shown in Fig. 7(b), and the EDS maps shown in Fig. 7(c) reveals the elemental distribution in the peak-aged state. It can be seen that the precipitates are rich in Mg and Sm elements, while the aggregation of Sn is absent,

this agrees well with the results shown in Fig. 5. The above analysis confirms that the Sm-containing phases are the dominant strengthening precipitate phases in the peak-aged TE3 alloy.

To further identify the needle-like precipitates and determine their orientation relationship with α-Mg matrix in the peak-aged TE3 alloy, TEM observations and selected area electron diffraction (SAED) viewed along the $[1\bar{1}0\bar{1}]_{\alpha\text{-Mg}}$ zone axis were carried out, as shown in Fig. 8. Based on the corresponding SAED patterns shown in Fig. 8(b), it can be concluded that the needle-like precipitate is $Mg_3Sm$ phase, and the structure of $Mg_3Sm$ is face-centered cubic with lattice parameter $a$=0.736 nm. The orientation relationship between $Mg_3Sm$ and α-Mg matrix is summarized as follows: $[1\bar{1}0\bar{1}]_{\alpha\text{-Mg}}//[001]_{Mg_3Sm}$ and $(10\bar{1}1)_{\alpha\text{-Mg}}//(220)_{Mg_3Sm}$. This observation result is consistant with the results of recent study in the binary Mg-Sm alloys [23, 24]. It has been reported that $Mg_3Sm$ intermediate phase has a significant strengthening effect on the Mg-Sm alloys during isothermal ageing process. Since hardness represents the ability to resist localized plastic deformation of alloys, it is reasonable to suggest that the significant hardness increment of peak-aged TE3 alloy in present study mainly originates from the precipitation of dispersive $Mg_3Sm$ phase, which are the effective obstacles to the motion of dislocations during localized plastic deformation, hence, a superior hardness value is achieved in the peak-aged TE3 alloy.

## 4 Conclusions

(1) Increasing the Sm/Sn ratio (0–2.55, in wt.%) in the experimental Mg-Sn-Sm alloy results in the formation of $Mg_{41}Sm_5$ and thermally stable MgSnSm phases, in addition, the solubility of Sn in α-Mg matrix decreases in the solution-treated samples. When the Sm/Sn ratio is about 1.19, the secondary dendrite arm spacing of α-Mg grains decreases significantly.

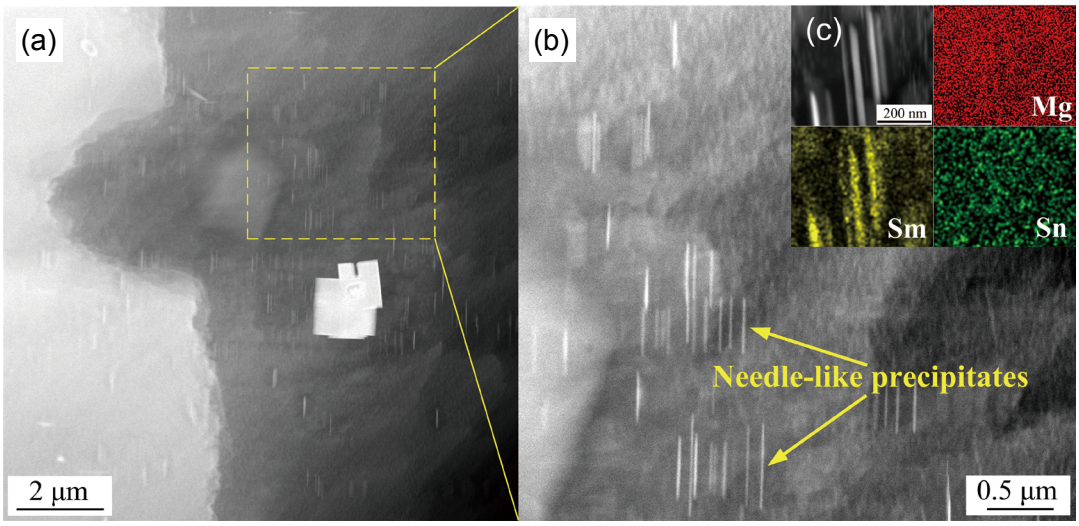


**Fig. 7: HAADF-STEM images of peak-aged TE3 alloy: (a) needle-like precipitates within α-Mg matrix; (b) magnified image of precipitates in (a); (c) EDS maps showing the chemical compositions of needle-like precipitates in (b)**

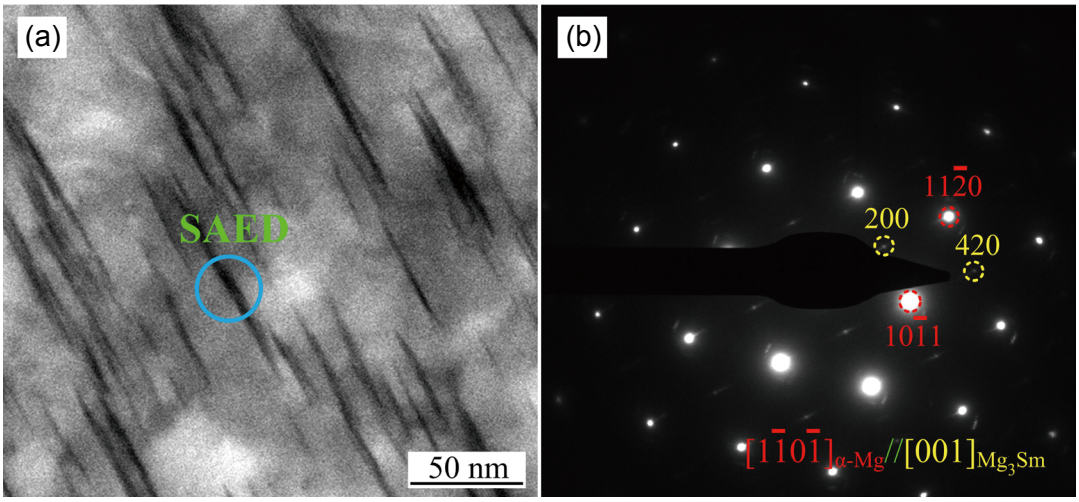


**Fig. 8: TEM bright field image and corresponding SAED pattern of peak-aged TE3 alloy: (a) bright field TEM image; (b) corresponding SAED patterns for the precipitates. The electron beam is parallel to the $[1\bar{1}0\bar{1}]_{\alpha\text{-Mg}}$**

(2) The age-hardening behavior of Mg-Sn-Sm alloy is significantly influenced by the Sm/Sn ratio. A high percentage of Sm element is consumed to form the thermally stable $Mg_x$(SnSm) or MgSnSm compounds in the TE1 and TE2 alloys during solidification, which weakens the ageing-hardening response.

(3) The large volume fraction of needle-like $Mg_3Sm$ precipitates contributes to the remarkable enhancement of hardness in the TE3 alloy. The orientation relationship between $Mg_3Sm$ and α-Mg matrix is summarized as follows: $[1\bar{1}0\bar{1}]_{\alpha\text{-Mg}}//[001]_{Mg_3Sm}$ and $(10\bar{1}1)_{\alpha\text{-Mg}}//(220)_{Mg_3Sm}$.

## Acknowledgements

This work was financially supported by the Natural Science Foundation of Inner Mongolia under Grant No. 2020MS05014, and the Science and Technology Planning of Inner Mongolia under Grant No. 2020GG0318.

## References

[1] Song J F, She J, Chen D L, et al. Latest research advances on magnesium and magnesium alloys worldwide. Journal of Magnesium and Alloys, 2020, 8: 1–41.
[2] Gavras S, Zhu S M, Nie J F, et al. On the microstructural factors affecting creep resistance of die-cast Mg-La-rare earth (Nd, Y or Gd) alloys. Materials Science and Engineering A, 2016, 675: 65–75.
[3] Liu C Q, Chen H W, Nie J F. Interphase boundary segregation of Zn in Mg-Sn-Zn alloys. Scripta Materialia, 2016, 123: 5–8.
[4] Pan F S, Yang M B, Chen X H. A review on casting magnesium alloys: Modification of commercial alloys and development of new alloys. Journal of Materials Science and Technology, 2016, 32: 1211–1221.
[5] Liu C Q, Chen H W, Liu H, et al. Metastable precipitate phases in Mg-9.8 wt%Sn alloy. Acta Materialia, 2018, 144: 590–600.
[6] Narreri G, Mahmudi R. Effects of Ca additions on the microstructural stability and mechanical properties of Mg-5%Sn alloy. Materials and Design, 2011, 32: 1571–1576.
[7] Li W D, Huang X F, Huang W G. Effects of Ca, Ag addition on the microstructure and age-hardening behavior of a Mg-7Sn (wt.%) alloy. Materials Science and Engineering A, 2017, 692: 75–80.
[8] Muthuraja C, Akalya A, Ahmed R R, et al. Experimental investigation and thermodynamic calculation of the phase equilibria in the Mg-rich region of Mg-Sn-Y alloys. Journal of Alloys and Compounds, 2017, 695: 3559–3572.
[9] Yang M B, Pan F S, Cheng L, et al. Effects of cerium on as-cast microstructure and mechanical properties of Mg-3Sn-2Ca magnesium alloy. Materials Science and Engineering A, 2009, 512: 132–138.
[10] Yang M B, Pan F S. Effects of Y addition on as-cast microstructure and mechanical properties of Mg-3Sn-2Ca (wt.%) magnesium alloy. Materials Science and Engineering A, 2009, 525: 112–120.
[11] Yang M B, Zhu Y, Liang X F, et al. Effects of Gd addition on as-cast microstructure and mechanical properties of Mg-3Sn-2Ca magnesium alloy. Materials Science and Engineering A, 2011, 528: 1721–1726.
[12] Chen Y A, Wang Y, Gao J J. Microstructure and mechanical properties of as-cast Mg-Sn- Zn-Y alloys. Journal of Alloys and Compounds, 2018, 740: 727–734.
[13] Wang P Q, Guo E Y, Wang X J, et al. The influence of Sc addition on microstructure and tensile mechanical properties of Mg-4.5Sn-5Zn alloys. Journal of Magnesium and Alloys, 2019, 7: 456–465.
[14] Xia X Y, Sun W H, Luo A A, et al. Precipitation evolution and hardening in Mg-Sm-Zn-Zr alloys. Acta Materialia, 2016, 111: 335–347.
[15] Zhang Y, Huang X F, Li Y, et al. Effects of samarium addition on as-cast microstructure, grain refinement and mechanical properties of Mg-6Zn-0.4Zr magnesium alloy. Journal of Rare Earths, 2017, 35: 494–502.
[16] Yu H S, Guo X F, Cui H B. Microstructures and tensile properties of as-cast Mg-5Sn-1Si magnesium alloy modified with trace elements of Y, Bi, Sb and Sr. China Foundry, 2021, 18(1): 9–17.
[17] Ali Y, Qiu D, Jiang B, et al. Current research progress in grain refinement of cast magnesium alloys: A review article. Journal of Alloys and Compounds, 2015, 619: 639–651.
[18] Kozlov O A, Grobner J, Schmid F R. Phase formation in Mg-Sn alloys modified by Ca and Ce. Journal of Phase Equilibria and Diffusion, 2014, 35: 502–517.
[19] Wang Q, Chen Y G, Xiao S F, et al. Study on microstructure and mechanical properties of as-cast Mg-Sn-Nd alloys. Journal of Rare Earths, 2010, 28: 790–793.
[20] Yang M B, Hou M D, Zhang J, et al. Effects of Ce, Y and Gd additions on as-cast microstructure and mechanical properties of Mg-3Sn-2Sr magnesium alloy. Transactions of Nonferrous Metals Society of China, 2014, 24: 2497–2506.
[21] Sasaki T T, Ohishi K, Ohkubo T, et al. Enhanced age hardening response by the addition of Zn in Mg-Sn alloys. Scripta Materialia, 2006, 55(2): 251–254.
[22] Mendis C L, Bettle C J, Gibson M A, et al. An enhanced age hardening response in Mg-Sn based alloys containing Zn. Materials Science and Engineering A, 2006, 435: 163–171.
[23] Zheng J X, Zhou W M, Chen B. Precipitation in Mg-Sm binary alloy during isothermal ageing: Atomic-scale insights from scanning transmission electron microscopy. Materials Science and Engineering A, 2016, 669: 304–311.
[24] Xie H B, Liu B S, Bai J Y, et al. Re-recognition of the aging precipitation behavior in the Mg-Sm binary alloy. Journal of Alloys and Compounds, 2020, 814: 1–6.